Biomedicine & Pharmacotherapy 145 (2022) 112426

Contents lists available at ScienceDirect

Biomedicine & Pharmacotherapy

journal homepage: www.elsevier.com/locate/biopha

Membrane model as key tool in the study of glutathione-s-transferase mediated anticancer drug resistance

Elsa M. Materón [a,b,*], Flavio M. Shimizu [b,c,*], Kevin Figueiredo dos Santos [b], Gustavo F. Nascimento [b], Vananélia P.N. Geraldo [b], Osvaldo N. Oliveira Jr [b,**], Ronaldo C. Faria [a,**]

[a] Chemistry Department, Federal University of São Carlos, CP 676, São Carlos 13565-905, São Paulo, Brazil
[b] São Carlos Institute of Physics, University of São Paulo, P.O Box 369, 13560-970 São Carlos, SP, Brazil
[c] Department of Applied Physics, "Gleb Wataghin" Institute of Physics (IFGW), University of Campinas (UNICAMP), Campinas, SP 13083-859, Brazil

ARTICLE INFO

Keywords:
Membrane model
Langmuir monolayer
Cisplatin
Doxorubicin
Detoxification enzyme
Glutathione-s-transferase

ABSTRACT

Glutathione-s-transferase is believed to be involved in the resistance to chemotherapeutic drugs, which depends on the interaction with the cell membranes. In this study, we employed Langmuir monolayers of a mixture of phospholipids and cholesterol (MIX) as models for tumor cell membranes and investigated their interaction with the anticancer drugs cisplatin (CDDP) and doxorubicin (DOX). We found that both DOX and CDDP expand and affect the elasticity of MIX monolayers, but these effects are hindered when glutathione-s-transferase (GST) and its cofactor glutathione (GSH) are incorporated. Changes are induced by DOX or CDDP on the polarization-modulated infrared reflection absorption spectroscopy (PM-IRRAS) data for MIX/GST/GSH monolayers, thus denoting some degree of interaction that is not sufficient to alter the monolayer mechanical properties. Overall, the results presented here give support to the hypothesis of the inactivation of DOX and CDDP by GST and point to possible directions to detect and fight drug resistance.

1. Introduction

The combination of chemotherapeutic drugs may bring synergistic effects and decrease the chances of drug resistance [1], but this requires the determination of pharmacokinetic profiles and biodistributions which is difficult to achieve [2]. This type of study is worth pursuing to reach an efficient chemotherapy, with less collateral effects and improved patient life quality [3]. For instance, the anticancer drugs doxorubicin (DOX) and cisplatin (CDDP) have been administered in "cocktail" chemotherapy with success for patients with malignant fibrous histiocytoma of bones, osteosarcoma [4], breast, ovarian, bladder, and various pediatric cancers [2]. CDDP is a metal-based drug administered intravenously with a sterile saline solution [5] to induce tumor cell apoptosis through the binding of DNA and formation of DNA adducts [3,6]. DOX acts directly on cancer cells through two mechanisms, namely inhibition of topoisomerase-II-mediated DNA repair and intercalation of DNA, and through damaging cell membranes via generation of free radicals [7]. These drugs combined have been used in phase III endometrial cancer patients, but side-effects like cardiotoxicity, myelosuppression, nausea, and vomiting have been reported [8,9], in addition to drug resistance [6,8,10,11]. A proposed mechanism of drug resistance in the cytoplasm is related to the glutathione (GSH) conjugation with CDDP in human lung carcinoma A549 cells by glutathione-s-transferase (GST) [12]. The complex of GSH and CDDP is excreted by GS-conjugated export pumps [5,13–16]. On the other hand, GSH levels are reduced in rat liver when exposed to DOX owing to increased detoxification with the elimination of reactive oxygen species [17,18] and resistance in Hep2 cells [19,20].

Drug resistance may be associated with membrane interactions, which may be investigated using living cells and functional read-out methods [21,22]. These methodologies have experimental limitations such as long-term experiments and high cost. Furthermore, the methods are non-specific for drug membrane interactions, and it is challenging to obtain molecular-level information. An elegant alternative is to use cell

* Corresponding authors at: Chemistry Department, Federal University of São Carlos, CP 676, São Carlos 13565-905, São Paulo, Brazil.
** Corresponding authors.
E-mail addresses: elsa_materon@yahoo.com (E.M. Materón), fshimizu@unicamp.br (F.M. Shimizu), chu@ifsc.usp.br (O.N. Oliveira Jr), rcfaria@ufscar.br (R.C. Faria).

https://doi.org/10.1016/j.biopha.2021.112426
Received 13 September 2021; Received in revised form 5 November 2021; Accepted 12 November 2021
Available online 30 November 2021

membrane models, including Langmuir monolayers with which molecular-level information can be obtained [21]. Such information can then be used to compare with the literature, not only related to cell membranes but also to various topics in molecular biology. DNA/lipid interactions in these monolayers have been crucial for developing DNA-based pharmaceuticals for gene therapy, biosensors, and nanodevices [23,24]. Many drugs, including the anesthetics lidocaine, prilocaine, mepivacaine, and ropivacaine have been studied in membrane models of cardiovascular and nervous systems [25] where changes in membrane fluidity were correlated to drug effects. Antimicrobial peptides [26] and proteins [27,28] have also been investigated with Langmuir monolayers. One of the main challenges in obtaining more realistic models is in the choice of the lipids comprising the Langmuir monolayers, for lipid composition varies according to organs, animals, and pathologies [23]. Cell membranes in breast tissue, for example, have altered fatty acid and phospholipidic profiles in tumor areas compared to healthy areas [29]. Changes in phospholipid composition may occur before morphological tumoral modifications and be related to the tumor malignancy [29–32].

In this study, we chose Langmuir monolayers as models of tumor cell membranes with the mixture of 1,2-dipalmitoyl-sn-glycero-3-phosphocholine (DPPC), 1,2-dipalmitoyl-sn-glycero-3-phosphoethanolamine (DPPE), 1,2-dipalmitoyl-sn-glycero-3-phospho-L-serine (DPPS), and cholesterol (Chol). The composition referred to as MIX has a proportion of 70:24:4:2 mol% for the molecules above, and was selected based on previous studies showing that DPPS is on the outer leaflet of cancer cell membranes [33–35]. The subphase in the Langmuir trough consisted of 0.1 mol/L phosphate buffer at pH 6.5 which mimics the slightly acidic microenvironment of tumors (pH 5.6–6.8) due to glycolysis in tumor cells contributing to drug resistance [36,37]. We investigated the interaction of DOX or CDDP with MIX Langmuir monolayers via a few experimental techniques, and how these interactions were affected by the presence of GST/GSH conjugates. The main aim was to verify whether the action of the drugs could be inhibited by GST/GSH, as hypothesized in the literature [15,19,38,39].

2. Materials and methods

1,2-dipalmitoyl-sn-glycero-3-phosphocholine (DPPC), 1,2-dipalmitoyl-sn-glycero-3-phosphoethanolamine (DPPE), 1,2-dipalmitoyl-sn-glycero-3-phospho-L-serine (DPPS) and cholesterol (Chol) were obtained from Avanti Polar Lipids, Inc. (Alabaster, AL, USA). Glutathione (GSH), glutathione-S-transferase from the equine liver (GST), doxorubicin hydrochloride (DOX), 1-chloro-2,4-dinitrobenzene, phosphate buffer saline pH 7.4, and Cisplatin (CDDP, European Pharmacopoeia standard) were purchased from Sigma Aldrich Co. (St. Louis, MO, USA) and United State Pharmacopeia (Rockville, MD, USA), respectively. The reagents, chloroform, ethanol, methanol, NaH_2PO_4, and Na_2HPO_4 were obtained from Synth (≥99.0%, Brazil). The aqueous solutions were prepared with ultrapure water (Milli-Q UV Plus system, Millipore Corp.) with a resistivity of 18.2 MΩ cm at 25 °C.

2.1. Langmuir films

The experiments were performed using a Langmuir minitrough (KSV-NIMA, area = 15,900 mm^2). The subphase contained 60 mL of 0.1 mol/L phosphate buffer solution at pH 6.5. The composition of the cancerous membrane model had 70 mol% dipalmitoyl phosphatidylcholine (DPPC, dissolved in chloroform), 24% phosphatidyl ethanolamine (DPPE, dissolved in 3:2 chloroform/ethanol), 4% dipalmitoyl phosphatidylserine (DPPS, dissolved in 3:2 chloroform/methanol), and 2% cholesterol (CHOL, dissolved in chloroform). Surface pressure (π) vs. mean molecular area (A) isotherms were recorded in triplicate by spreading 10 μL of the lipid mixture on the air-buffer interface. After 15 min for solvent evaporation and stabilization of the monolayer, the barriers were symmetrically compressed at a rate of 10 mm/min, and the Wilhelmy method was used to measure the surface pressure. The Langmuir trough was cleaned with chloroform and ultrapure water. All experiments were performed in a class 10,000 cleanroom at 22 ± 1 ℃. Typically, a lipid monolayer is spread from an organic solvent to the desired surface pressure and the protein of interest is injected under the monolayer and allowed to interact with it [40,41]. We spread the mixture of lipids onto the subphase surface using a microsyringe, and 15 min later (time required for the chloroform evaporate) the protein was added to the subphase (~60 mL for the minitrough used in this study, Fig. 1). The π-A isotherms were made in triplicate (n = 3).

2.2. Compressional modulus

The monolayer stiffness was assessed by analyzing the compressibility modulus, Cs^{-1}, calculated from the isotherm (π-A)

$$C_s^{-1} = -A\frac{d\pi}{dA}$$

where A is the average area per molecule at a given surface pressure π.

2.3. Adsorption kinetics

Adsorption kinetics studies were performed according to the procedure depicted in Fig. S1. Firstly, the cancerous membrane model (MIX) was formed on the 0.1 mol/L phosphate buffer pH 6.5 subphase of the Langmuir minitrough. A waiting time of 15 min was allowed for solvent evaporation. Then GST enzyme (3.3 mg/mL, 10 μL) and GSH (5 mmol/L, 300 μL) cofactor were sequentially injected in the subphase. Between each step, the surface pressure was recorded for 30 min. For the drug studies, a waiting time of 60 min was established to allow for a steady-state condition for the MIX/GST/GSH membrane, after which CDDP (4.5 mmol/L, 300 μL) or DOX (4.5 mmol/L, 300 μL) was injected into the subphase. The surface pressure was then recorded for 60 min

2.4. PM-IRRAS

Langmuir films were compressed at 30 mN/m in a Langmuir KSV Nima minitrough and the PM-IRRAS spectra were obtained using a KSV PMI 550 spectrometer (KSV Instruments, Helsinki, Finland). All measurements were performed with the incident beam at 81° so that positive bands correspond to the parallel orientation of the chemical groups at the air-buffer interface [42]. The PM-IRRAS (S) signal is given by:

$$S = \frac{R_p - R_s}{R_p + R_s}$$

where R_p and R_s are the polarized reflectances in parallel (p) and perpendicular (s), respectively, to the incidence plane. The spectral range is 800–4000 cm^{-1} and the spectral resolution is 8 cm^{-1}. PM-IRRAS measurements were made in duplicate (n = 2).

2.5. BAM

The enzymatic solution was injected under the monolayer in the same way as during PM-IRRAS and isotherm experiments using a Brewster angle microscope (BAM), BAM2 plus microscope (Nanofilm EP4 Technology Germany). The images were acquired at the surface pressure of 30 mN/m.

3. Results and discussion

3.1. GST/membrane model interactions

GST enzymes catalyze the reaction in which glutathione (GSH) is conjugated with various exogenous and endogenous xenobiotics. Conjugation occurs firstly via the mercapturic acid pathway, then

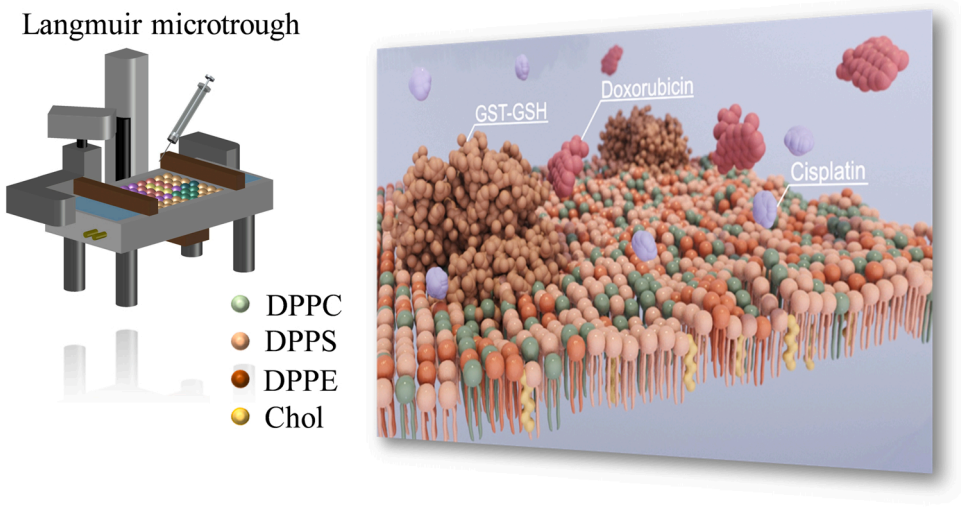

Fig. 1. Schematic design of the minitrough with the membrane model and GST/GSH in the subphase.

inducing the elimination of toxic compounds from the cell [43]. GSTs have two active sites, viz. a hydrophilic G-site for GSH binding, and a hydrophobic H-site for the binding of structurally-different electrophilic substrates (e.g. anticancer drugs) [44]. For this reason, we investigated the incorporation of GST and its cofactor GSH in the monolayer representing a cancerous membrane model (MIX). The surface pressure-area isotherms for neat lipid components (DPPC, DPPE, DPPS, and CHOL), MIX, and MIX/GSH control are given in Fig. S2 in the Supporting Information. As expected, the addition of GSH did not alter the isotherm. In our experiments, after spreading the mixture of lipids onto the subphase using a microsyringe we waited for the complete evaporation of solvents to then inject 10 μL of the enzymatic stock solution at 3.3 mg/mL in phosphate-buffered saline pH 7.4 into 60 mL of 0.1 mol/L phosphate buffer pH 6.5 subphase in the Langmuir minitrough. Nobre et al. [35] studied the methodologies for adding proteins to a Langmuir film and observed that spreading both components from the same solution yields more homogeneous films, but the organic solvent dissolving the lipid could lead to dramatic, irreversible changes in protein

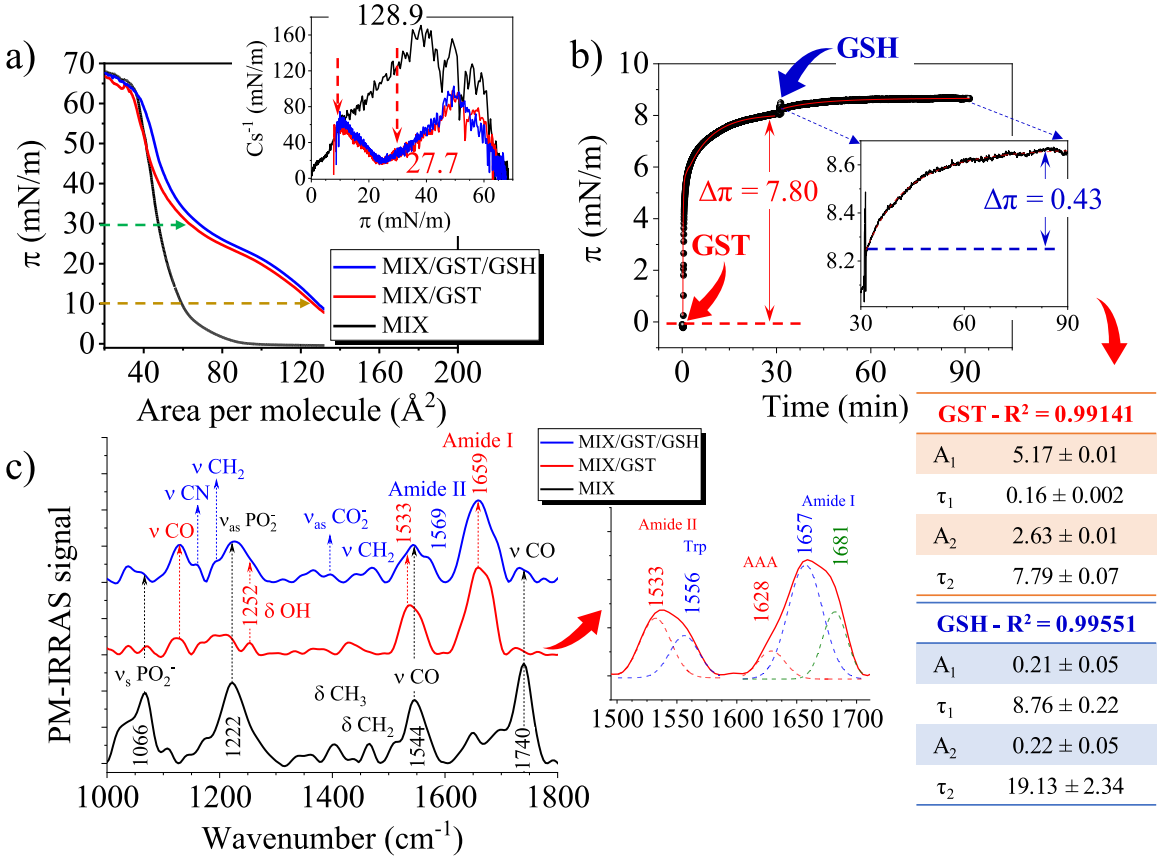

Fig. 2. a) π-A isotherms for the MIX monolayer, including in the presence of GST and GST/GSH, with the compressibility modulus in the inset. b) adsorption kinetics with π vs. time for MIX as GST and GSH are added. C) PM-IRRAS spectra for the neat MIX monolayer and those incorporating GST and GSH at 30 mN/m.

structure. Fig. 2a presents the π-A isotherms for the membrane model (MIX) in the presence of GST enzyme (MIX/GST), and its cofactor (MIX/GST/GSH). Significant changes occur upon GST enzyme incorporation; more specifically, at 10 mN/m a liquid-expanded phase arises, and the area increases from 59.2 ± 0.7–126.8 ± 1.8 Å^2, with the compressibility modulus decreasing by ~10 mN/m. At the physiologically-relevant membrane pressure of 30 mN/m [25], i.e. in the liquid-condensed phase, the area per molecule increases from 47.5 ± 0.9–63.2 ± 2.0 Å^2. In addition, the membrane fluidity increased drastically as the compressibility modulus varied from 128.9 ± 8.9–27.7 ± 0.7 mN/m, which confirms the enzyme incorporation. A summary of isotherm analytical values from Fig. 2a is depicted in Table S1. The initial surface pressure of MIX/GST π-A isotherm does not start from zero. This was expected from the adsorption kinetics results in Fig. 2b, which feature a large increase in pressure and stabilization at ca. 7.8 mN/m upon adding GST. The adsorption kinetics could be fitted using a bi-exponential function, suggesting that GST incorporation occurs in two steps. The time constants were $\tau_1 = 0.16$ min and $\tau_2 = 7.79$ min, which means an initially fast adsorption followed by penetration that requires a longer time. The addition of the cofactor GSH to the GST/MIX membrane causes only slight changes in the π-A isotherm and negligible change in Cs^{-1} in Fig. 2a, which could be explained by the GSH small size and high specificity for the G-binding site [44]. These small alterations are consistent with the adsorption kinetics in Fig. 2b, where GSH incorporation caused a small increase of 0.43 mN/m in the pressure. Also, to be noted are the large time constants for the bi-exponential function to fit the data ($\tau_1 = 8.76$ min and $\tau_2 = 19.13$ min).

Information of molecular-level interactions [46] can be inferred from the PM-IRRAS spectra in Fig. 2c. The main vibrational bands from MIX

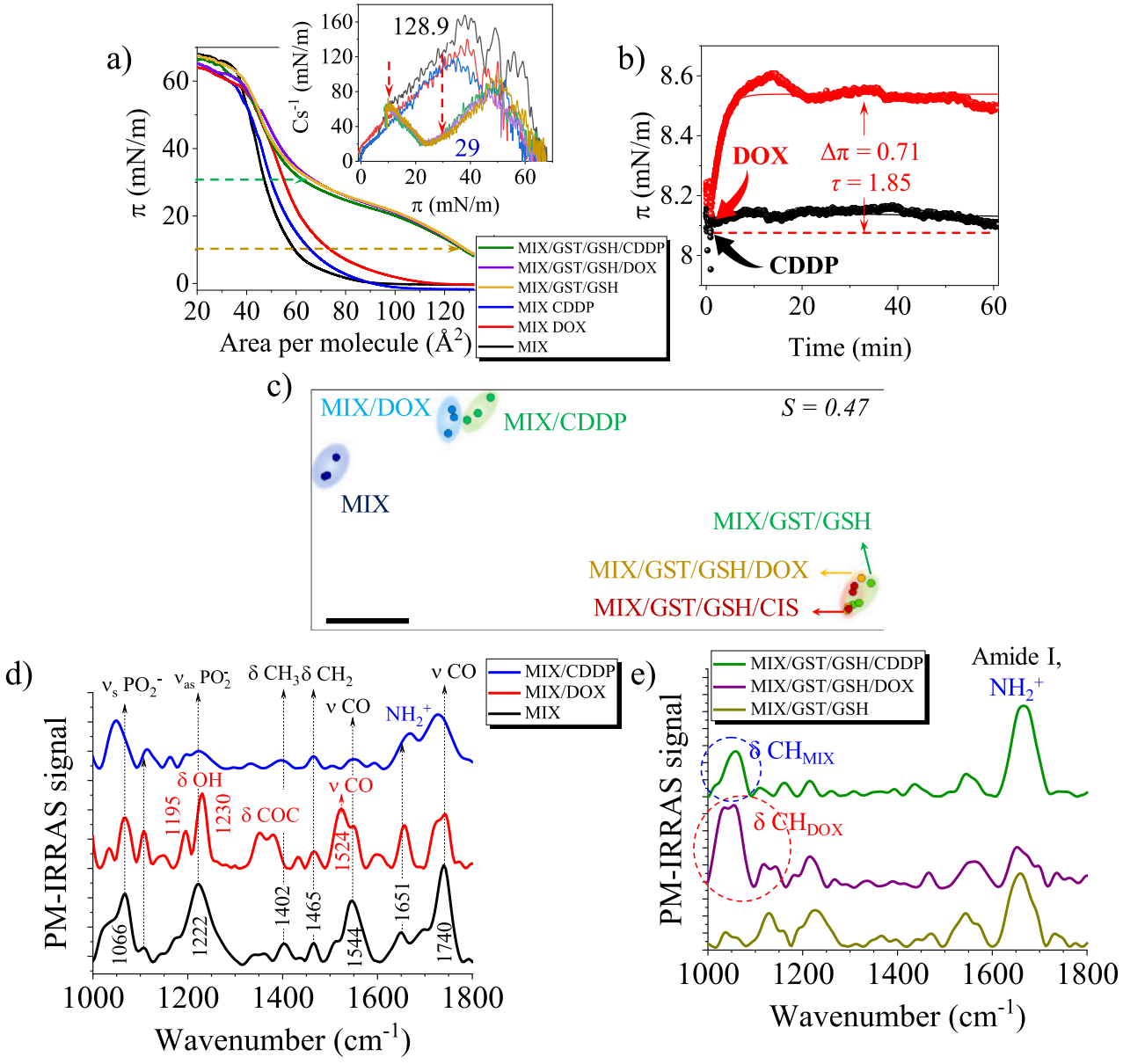

Fig. 3. a) π-A isotherms for MIX monolayers in the presence of GST and GSH cofactor (MIX/GST/GSH) and anticancer drugs (CDDP and DOX). Inset. Compressibility modulus/surface pressure (C_s^{-1}/π) of the membrane model (MIX), MIX/CDDP (black line), MIX/DOX (red line), MIX/GST/GSH (purple), MIX/GST/GSH/CDDP (blue line), MIX/GST/GSH/DOX (green line). b). Changes in surface pressure along time for the MIX/GST/GSH monolayer upon the incorporation of DOX (red line, 90 min) and CDDP (black line, 90 min). c) IDMAP plot of all π-A isotherms from Fig. 3a in the pressure range of 9 – 30 mN/m. The black bar is for a reference guide only. d) PM-IRRAS spectra of MIX, including after addition of CDDP and DOX drugs. e) PM-IRRAS spectra of MIX in the presence of GST and GSH cofactor (MIX/GST/GSH) after addition of CDDP and DOX.

(spectrum in black) include the symmetric (ν_s) and asymmetric (ν_{as}) stretching of the PO_2^- group at 1066 and 1222 cm^{-1}, respectively, and CO stretching (ν CO) at 1544 and 1740 cm^{-1}. Upon adding GST (spectrum in red), relevant vibrational bands are suppressed, and others arise. The intensity of PO_2^- and CO bands from MIX decreased considerably, and GST incorporation is evidenced by new bands at 1128, 1252, 1533, and 1659 cm^{-1} assigned to CO stretching, OH bending, and amide II and I bands, respectively. The inset depicts the deconvolution of amide I and II bands from aromatic residues such as Phe, Tyr, and Trp [47]. Even though GSH had almost negligible effects on the π-A and C_s^{-1} - π isotherms, it induced a broadening of amide I and II bands and gave rise to the 1569 cm^{-1} band assigned to the CN stretching (spectrum in blue). Furthermore, the phosphate vibrational band which was suppressed by GST reappeared upon incorporating GSH. Large changes are observed in Fig. S3 in the Supporting Information for the 2800–3000 cm^{-1} region corresponding to the aliphatic chains. The symmetric and asymmetric CH stretching modes of CH_2 and CH_3 appear at 2856, 2915, 2954, and 2980 cm^{-1} for the three monolayers, viz. MIX, MIX/GST, and MIX/GST/GSH. The addition of GST caused configurational disorder in the chains as the ratio between the intensity of symmetric and asymmetric bands (I_s/I_{as}) increased from 0.37 to 1.0. Such disordering effect may be related to the increase in gauche conformers of lipid chains, inducing a decreased intensity of vibrational bands, a shift to lower wavenumbers, and the split of ν_{as} CH_2 band. GSH induced a split in ν (HC=CH) and $\nu_s CH_2$ bands, which leads to a decrease in I_s/I_{as} ratio to 0.76. These results mean that GSH interacts with MIX without affecting the surface pressure isotherms, probably because it is located below the interface.

3.2. Incorporation of DOX and CDDP in MIX monolayers with GST/GSH

The effects from DOX and CDDP at mmol/L on MIX monolayers are shown in Fig. 3a, with an expansion in the surface pressure isotherms. DOX and CDDP also caused a small decrease in the compressibility modulus as shown in the inset. In contrast, for the MIX/GST/GSH monolayer there is practically no effect from either DOX or CDDP. The changes in the isotherms in Fig. 3a are depicted in Table S1. This can be seen in the surface pressure isotherms and compressibility modulus data in Fig. 3a. In the adsorption kinetics in Fig. 3b, there is a small increase in pressure induced by DOX and almost no change with CDDP. Taken together these results appear to indicate that the action of DOX and CDDP on MIX is hindered in the presence of GST/GSH. This conclusion is consistent with the reaction mechanism in Figs. S4 and S5 in the Supplementary Information. It may be illustrated by employing the multidimensional projection technique interactive document mapping (IDMAP) to represent each surface pressure isotherm as a data point on a 2D map [48]. Indeed, the IDMAP plot in Fig. 3**c** confirms that DOX and CDDP induce considerable changes on MIX, with the corresponding data points being far from each other, while the points referring to MIX/GST/GSH is on the same cluster as the points for MIX/GST/GSH/DOX or MIX/GST/GSH/CDDP. The use of IDMAP is important here to show the statistical relevance of the differences observed.

The PM-IRRAS spectra in Fig. 3d confirm the considerable effects of DOX and CDDP on the MIX monolayer. New bands appear at 1195, 1230, 1351, 1381, and 1524 cm^{-1}, owing to the ring stretching of DOX with OH and COC bending and symmetric stretching of the CO group. The main vibrational bands of MIX are slightly changed by DOX, such as the well-defined phosphate bands at the region of 1000–1100 cm^{-1} and CO bands between 1500 and 1800 cm^{-1}. The penetration of DOX in the membrane model is confirmed by a decreased intensity of aliphatic bands and an increase in I_s/I_{as} ratio from 0.37 (MIX) to 0.72 (MIX/DOX) in Fig. S6a in the Supporting Information, which means an increased disorder in the aliphatic chains. Moreover, DOX induced a split in the $\nu_{as}CH_2$ band while the $\nu_{as}CH_3$ and ν(HC=CH) bands are merged into a single band at 2966 cm^{-1}. For CDDP only one vibrational band due to protonated amine group appears at 1669 cm^{-1}, but several bands assigned to MIX have their intensity decreased considerably and the PO_2 and CO bands are shifted to lower energies owing to the reorientation of the lipid molecules. Fig. S6a in the Supporting Information indicates that CDDP incorporation led to an increase in I_s/I_{as} ratio to 0.65, with a broader $\nu_{as}CH_2$ band. The addition of DOX or CDDP to the MIX/GST/GSH monolayer caused only small changes in the PM-IRRAS spectra in Fig. 3e, corresponding to the lipid headgroup region. The most significant change appears in the region between 1000 and 1200 cm^{-1} assigned to the bending of CH groups, possibly owing to the complexation of the drugs with GST/GSH. The other worth noting changes occur in the amide I band, with a decrease for MIX/GST/GSH/DOX and an increase for MIX/GST/GSH/CDDP. Large changes, however, are observed in the aliphatic chains between 2800 and 3000 cm^{-1} in Fig. S6b in the Supporting Information. The addition of DOX increased the intensity of $\nu_s CH_2$ and ν(HC=CH) bands, caused a split of the $\nu_{as}CH_2$ band to 2884 and 2908 cm^{-1}, and made the $\nu_{as}CH_3$ band disappear. An increase was observed in the I_s/I_{as} ratio from 0.76 (MIX/GST/GSH) to 1.30 (MIX/GST/GSH/DOX), which means a decrease in the ordering of lipids tails. For CDDP, ν_s and $\nu_{as}CH_2$ bands are split and the $\nu_{as}CH_3$ and ν (HC=CH) bands merged. The I_s/I_{as} ratio decreased to 0.49 which suggests an increase in the molecular ordering. The reason why DOX and CDDP affected the PM-IRRAS from MIX/GST/GSH monolayers, despite the lack of change in the surface pressure isotherms, may be the high sensitivity of this vibrational spectroscopy. Small changes in dipole orientation, for instance, can lead to changes in the monolayer PM-IRRAS spectrum, even if the drugs do not penetrate in the monolayer. Another sensitive technique to small changes at the interface is BAM, whose images in Fig. S7 in the Supporting Information also indicate that DOX and CDDP affect the MIX/GST/GSH monolayer with changes in morphology. CDDP and DOX alter the morphology of the lipid membrane with GST in different ways, and these effects could not be related directly to the isotherm results.

It is worth noting that in subsidiary experiments with various concentrations of DOX and CDDP, we observed that the MIX Langmuir monolayers were affected to different extents in Fig. S8 in the Supporting Information. From an IDMAP plot of the isotherms, we could distinguish drug concentrations even at 10^{-5} M, which suggests that Langmuir-Blodgett (LB) films deposited on solid supports from monolayers such as MIX may be employed as biosensors. GST could be immobilized in a biosensor to detect metabolites from the drugs [49].

4. Conclusions and biological implications

The anticancer drugs DOX and CDDP expanded the surface pressure isotherms of the MIX monolayer, also affecting their elasticity. This should be expected from the physiological action of these drugs and provides evidence that the MIX composition was appropriate to mimic a tumor cell membrane [35,50]. The effects from DOX or CDDP on the mechanical properties of MIX monolayers, however, were neutralized by incorporating GST and its cofactor GSH as observed with immunohistochemistry [51] and other techniques [52,53]. This does not mean that the interaction between DOX and CDDP has completely vanished; some interaction could be inferred from PM-IRRAS and BAM images. It seems that molecular-level interactions are only sufficient to generate action by the anticancer drugs if the elasticity and packing of the monolayers (i.e., membranes) are affected. This is consistent with the hypothesis of GST/GSH being linked to drug resistance. We also observed that the effects from DOX and CDDP are concentration dependent, which means that the MIX monolayer could be transferred as LB films and then be used in biosensors. Detection of GST levels in the blood could be related to the presence of drug resistance.

CRediT authorship contribution statement

E.M.M.: Conceptualization, Methodology, Investigation,

Visualization, Writing; F.M.S.: Formal analysis, Writing; K.F.: Methodology, Validation; G.F.N.: Methodology, Validation; V.P.N.G.: Methodology, Validation; O.N.O.Jr.: Conceptualization, Writing, Supervision, Resources; R.C.F. Conceptualization, Writing, Supervision.

Conflict of Interest Statement

The authors declare that they have no known competing financial interests or personal relationships that could have appeared to influence the work reported in this paper.

Acknowledgments

This work was supported by Sao Paulo Research Foundation (FAPESP) (2012/15543-7, 2016/00991-5, 2017/24053-7, and 2018/22214-6), Brazilian National Council for Scientific and Technological Development (CNPq), Ministry of Science, Technology and Inovation (MCTI-SisNano, Brazil).

Appendix A. Supporting information

Supplementary data associated with this article can be found in the online version at doi:10.1016/j.biopha.2021.112426.

References

[1] D.A. Yardley, Drug resistance and the role of combination chemotherapy in improving patient outcomes, Int. J. Breast Cancer 2013 (2013) 1–15, https://doi.org/10.1155/2013/137414.
[2] F. Lopes, J. Liu, S. Morgan, R. Matthews, L. Nevin, R.A. Anderson, N. Spears, Single and combined effects of cisplatin and doxorubicin on the human and mouse ovary in vitro, Reproduction 159 (2020) 193–204, https://doi.org/10.1530/REP-19-0279.
[3] H. Wu, H. Jin, C. Wang, Z. Zhang, H. Ruan, L. Sun, C. Yang, Y. Li, W. Qin, C. Wang, Synergistic cisplatin/doxorubicin combination chemotherapy for multidrug-resistant cancer via polymeric nanogels targeting delivery, ACS Appl. Mater. Interfaces 9 (2017) 9426–9436, https://doi.org/10.1021/acsami.6b16844.
[4] V.H.C. Bramwell, W.P. Steward, M. Nooij, J. Whelan, A.W. Craft, R.J. Grimer, A.H. M. Taminau, S.R. Cannon, A.J. Malcolm, P.C.W. Hogendoorn, B. Uscinska, A. L. Kirkpatrick, D. Machin, M.M.Van Glabbeke, Neoadjuvant chemotherapy with doxorubicin and cisplatin in malignant fibrous histiocytoma of bone: a European osteosarcoma intergroup study, J. Clin. Oncol. 17 (1999) 3260–3269, https://doi.org/10.1200/JCO.1999.17.10.3260.
[5] S. Ghosh, Cisplatin: the first metal based anticancer drug, Bioorg. Chem. 88 (2019), 102925, https://doi.org/10.1016/j.bioorg.2019.102925.
[6] K. Okamoto, Y. Saito, K. Narumi, A. Furugen, K. Iseki, M. Kobayashi, Different mechanisms of cisplatin resistance development in human lung cancer cells, Biochem. Biophys. Res. Commun. 530 (2020) 745–750, https://doi.org/10.1016/j.bbrc.2020.07.040.
[7] C.F. Thorn, C. Oshiro, S. Marsh, T. Hernandez-Boussard, H. McLeod, T.E. Klein, R. B. Altman, Doxorubicin pathways: pharmacodynamics and adverse effects, Pharm. Genom. 21 (2011) 440–446, https://doi.org/10.1097/fpc.0b013e32833ffb56.
[8] Y. Wang, J. Qian, M. Yang, W. Xu, J. Wang, G. Hou, L. Ji, A. Suo, Doxorubicin/cisplatin co-loaded hyaluronic acid/chitosan-based nanoparticles for in vitro synergistic combination chemotherapy of breast cancer, Carbohydr. Polym. 225 (2019), 115206, https://doi.org/10.1016/j.carbpol.2019.115206.
[9] O. Tacar, P. Sriamornsak, C.R. Dass, Doxorubicin: an update on anticancer molecular action, toxicity and novel drug delivery systems, J. Pharm. Pharmacol. 65 (2013) 157–170, https://doi.org/10.1111/j.2042-7158.2012.01567.x.
[10] W. Ma, L. Yang, H. Liu, P. Chen, H. Ren, P. Ren, PAXX is a novel target to overcome resistance to doxorubicin and cisplatin in osteosarcoma, Biochem. Biophys. Res. Commun. 521 (2020) 204–211, https://doi.org/10.1016/j.bbrc.2019.10.108.
[11] X. Song, X. Liu, W. Chi, Y. Liu, L. Wei, X. Wang, J. Yu, Hypoxia-induced resistance to cisplatin and doxorubicin in non-small cell lung cancer is inhibited by silencing of HIF-1α gene, Cancer Chemother. Pharmacol. 58 (2006) 776–784, https://doi.org/10.1007/s00280-006-0224-7.
[12] A. De Luca, L.J. Parker, W.H. Ang, C. Rodolfo, V. Gabbarini, N.C. Hancock, F. Palone, A.P. Mazzetti, L. Menin, C.J. Morton, M.W. Parker, M. Lo Bello, P. J. Dyson, A structure-based mechanism of cisplatin resistance mediated by glutathione transferase P1-1, Proc. Natl. Acad. Sci. USA 116 (2019) 13943–13951, https://doi.org/10.1073/pnas.1903297116.
[13] Z.Z. Huang, C. Chen, Z. Zeng, H. Yang, J. Oh, L. Chen, S.C. Lu, Mechanism and significance of increased glutathione level in human hepatocellular carcinoma and liver regeneration, FASEB J. 15 (2001) 19–21, https://doi.org/10.1096/fj.00-0445fje.
[14] V.J. Findlay, D.M. Townsend, 12 S -Transferases in Drug Resistance, (n.d.) 213–221.
[15] S. Jana, S. Mandlekar, Role of phase II drug metabolizing enzymes in cancer chemoprevention, Curr. Drug Metab. 10 (2009) 595–616, https://doi.org/10.2174/138920009789375379.
[16] B. Stordal, M. Davey, Understanding cisplatin resistance using cellular models, IUBMB Life 59 (2007) 696–699, https://doi.org/10.1080/15216540701636287.
[17] P.L. Prasanna, K. Renu, A. Valsala Gopalakrishnan, New molecular and biochemical insights of doxorubicin-induced hepatotoxicity, Life Sci. 250 (2020), 117599, https://doi.org/10.1016/j.lfs.2020.117599.
[18] T. Asakura, K. Ohkawa, N. Takahashi, K. Takada, T. Inoue, S. Yokoyama, Glutathione-doxorubicin conjugate expresses potent cytotoxicity by suppression of glutathione S-transferase activity: Comparison between doxorubicin-sensitive and -resistant rat hepatoma cells, Br. J. Cancer 76 (1997) 1333–1337, https://doi.org/10.1038/bjc.1997.557.
[19] A. Harbottle, A.K. Daly, K. Atherton, F.C. Campbell, Role of glutathione S-transferase P1, P-glycoprotein and multidrug resistance-associated protein 1 in acquired doxorubicin resistance, Int. J. Cancer 92 (2001) 777–783, https://doi.org/10.1002/ijc.1283.
[20] E. Drozd, B. Gruber, J. Marczewska, J. Drozd, E. Anuszewska, Intracellular glutathione level and efflux in human melanoma and cervical cancer cells differing in doxorubicin resistance, Post. Hig. Med. Dosw. 70 (2016) 319–328, https://doi.org/10.5604/17322693.1199712.
[21] A.I. Bunea, S. Harloff-Helleberg, R. Taboryski, H.M. Nielsen, Membrane interactions in drug delivery: Model cell membranes and orthogonal techniques, Adv. Colloid Interface Sci. 281 (2020), https://doi.org/10.1016/j.cis.2020.102177.
[22] T.H. Lee, V. Hofferek, F. Separovic, G.E. Reid, M.I. Aguilar, The role of bacterial lipid diversity and membrane properties in modulating antimicrobial peptide activity and drug resistance, Curr. Opin. Chem. Biol. 52 (2019) 85–92, https://doi.org/10.1016/j.cbpa.2019.05.025.
[23] C. Stefaniu, G. Brezesinski, H. Möhwald, Langmuir monolayers as models to study processes at membrane surfaces, Adv. Colloid Interface Sci. 208 (2014) 197–213, https://doi.org/10.1016/j.cis.2014.02.013.
[24] M.N. Antipina, I. Schulze, M. Heinze, B. Dobner, A. Langner, G. Brezesinski, Physical-chemical properties and transfection activity of cationic Lipid/DNA complexes, ChemPhysChem 10 (2009) 2471–2479, https://doi.org/10.1002/cphc.200900069.
[25] J. Mildner, A. Wnętrzak, P. Dynarowicz-Latka, Cholesterol and cardiolipin importance in local anesthetics–membrane interactions: the Langmuir monolayer study, J. Membr. Biol. 252 (2019) 31–39, https://doi.org/10.1007/s00232-018-0055-6.
[26] T. Keszthelyi, K. Hill, É. Kiss, Interaction of phospholipid langmuir monolayers with an antibiotic peptide conjugate, J. Phys. Chem. B. 117 (2013) 6969–6979, https://doi.org/10.1021/jp401533c.
[27] A. Chachaj-Brekiesz, A. Wnętrzak, S. Włodarska, E. Lipiec, P. Dynarowicz-Latka, Molecular insight into neurodegeneration – Langmuir monolayer study on the influence of oxysterols on model myelin sheath, J. Steroid Biochem. Mol. Biol. 202 (2020), 105727, https://doi.org/10.1016/j.jsbmb.2020.105727.
[28] A. Junghans, C. Champagne, P. Cayot, C. Loupiac, I. Köper, Protein-lipid interactions at the air-water interface, Langmuir 26 (2010) 12049–12053, https://doi.org/10.1021/la100036v.
[29] V. Lladó, D.J. López, M. Ibarguren, M. Alonso, J.B. Soriano, P.V. Escribá, X. Busquets, Regulation of the cancer cell membrane lipid composition by NaCHOleate: Effects on cell signaling and therapeutical relevance in glioma, Biochim. Biophys Acta Biomembr. 1838 (2014) 1619–1627, doi:10.1016/j.bbamem.2014.01.027.
[30] S.R. Nagarajan, L.M. Butler, A.J. Hoy, The diversity and breadth of cancer cell fatty acid metabolism, Cancer Metab. 9 (2021) 1–28, https://doi.org/10.1186/s40170-020-00237-2.
[31] G. Van Meer, I.P.M. Anton, G. Van Meer, A.I.P.M.De Kroon, Lipid map of the mammalian cell Lipid Map of the Mammalian Cell, J. Cell Sci. 124 (2011) 5–8, https://doi.org/10.1242/jcs.071233.
[32] H.I. Ingo, M.N. Melo, F.J. Van Eerden, C.A. Lopez, T.A. Wassenaar, X. Periole, A. H. De Vries, D.P. Tieleman, S.J. Marrink, Lipid organization of the plasma membrane, J. Am. Chem. Soc. 136 (2014) 14554–14559.
[33] A.C. Alves, D. Ribeiro, M. Horta, J.L.F.C. Lima, C. Nunes, S. Reis, The daunorubicin interplay with mimetic model membranes of cancer cells: a biophysical interpretation, Biochim. Biophys. Acta Biomembr. 1859 (2017) 941–948, https://doi.org/10.1016/j.bbamem.2017.01.034.
[34] C. Wodlej, S. Riedl, B. Rinner, R. Leber, C. Drechsler, D.R. Voelker, J.Y. Choi, K. Lohner, D. Zweytick, Interaction of two antitumor peptides with membrane lipids - Influence of phosphatidylserine and cholesterol on specificity for melanoma cells, PLoS One 14 (2019), e0211187, https://doi.org/10.1371/journal.pone.0211187.
[35] T.M. Nobre, F.J. Pavinatto, L. Caseli, A. Barros-timmons, P. Dynarowicz-Łatka, O. N. Oliveira Jr, Interactions of bioactive molecules & nanomaterials with Langmuir monolayers as cell membrane models, Thin Solid Films 593 (2015) 158–188, https://doi.org/10.1016/j.tsf.2015.09.047.
[36] E.S. Lee, Y.H. Bae, Recent progress in tumor pH targeting nanotechnology, J. Control Release 132 (2009) 164–170, https://doi.org/10.1016/j.jconrel.2008.05.003.Recent.
[37] B. Lin, H. Chen, D. Liang, W. Lin, X. Qi, H. Liu, X. Deng, Acidic pH and high - H2O2 dual tumor microenvironment-responsive nanocatalytic graphene oxide for cancer selective therapy and recognition, ACS Appl. Bio Mater. 11 (2019) 11157–11166, https://doi.org/10.1021/acsami.8b22487.

[38] D.M. Townsend, K.D. Tew, The role of glutathione-S-transferase in anti-cancer drug resistance, Oncogene 22 (2003) 7369–7375, https://doi.org/10.1038/sj.onc.1206940.
[39] S. Ran, P.E. Thorpe, Phosphatidylserine is a marker of tumor vasculature and a potential target for cancer imaging and therapy, Int. J. Radiat. Oncol. Biol. Phys. 54 (2002) 1479–1484, https://doi.org/10.1016/S0360-3016(02)03928-7.
[40] H. Brockman, Lipid monolayers: why use half a membrane interactions? Curr. Opin. Struct. Biol. 9 (1999) 438–443.
[41] W.R. Glomm, S. Volden, Ø. Halskau, M.-H.G. Ese, Same system−different results: the importance of protein-introduction protocols in langmuir-monolayer studies of lipid-protein interactions, Anal. Chem. 81 (2009) 3042–3050, https://doi.org/10.1021/ac8027257.
[42] R.F. Vázquez, M.A.D. Millone, F.J. Pavinatto, M.L. Fanani, O.N.O. Jr, M.E. Vela, S. M. Maté, PII:, Impact of sphingomyelin acyl chain (16:0 vs 24:1) on the interfacial properties of Langmuir monolayers: a PM-IRRAS study, Colloids Surf. B Biointerfaces (2018) 1–20, https://doi.org/10.1016/j.colsurfb.2018.10.018.
[43] G.K.S.K. Gupta, P.S.V. Ali, V.K.M. Verma, Drug - metabolizing enzymes: role in drug resistance in cancer, Clin. Transl. Oncol. 22 (2020) 1667–1680, https://doi.org/10.1007/s12094-020-02325-7.
[44] N. Allocati, M. Masulli, C. Di Ilio, L. Federici, Glutathione transferases: substrates, inihibitors and pro-drugs in cancer and neurodegenerative diseases, Oncogenesis 7 (2018) 8, https://doi.org/10.1038/s41389-017-0025-3.
[46] M. Krajewska, K. Dopierała, P. Wydro, M. Broniatowski, K. Prochaska, Interfacial complex of α-lactalbumin with oleic acid: effect of protein concentration and PM-IRRAS study, J. Mol. Liq. 319 (2020), https://doi.org/10.1016/j.molliq.2020.114089.
[47] A. Rygula, K. Majzner, K.M. Marzec, A. Kaczor, M. Pilarczyk, M. Baranska, Raman spectroscopy of proteins: a review, J. Raman Spectrosc. 44 (2013) 1061–1076, https://doi.org/10.1002/jrs.4335.
[48] R. Minghim, F.V. Paulovich, A. de Andrade Lopes, Content-based text mapping using multi-dimensional projections for exploration of document collections, Vis. Data Anal. 2006 (6060) (2006) 60600S, https://doi.org/10.1117/12.650880.
[49] E.M. Materon, P.J. Jimmy Huang, A. Wong, A.A. Pupim Ferreira, M.D.P. T. Sotomayor, J. Liu, Glutathione-s-transferase modified electrodes for detecting anticancer drugs, Biosens. Bioelectron. 58 (2014) 232–236, https://doi.org/10.1016/j.bios.2014.02.070.
[50] E.M. Materon, G.F. Nascimento, F.M. Shimizu, A.S. Câmara, B. Sandrino, R. C. Faria, O.N. Oliveira Jr, Role of sphingomyelin on the interaction of the anticancer drug gemcitabine hydrochloride with cell membrane models, Colloids Surf. B Biointerfaces 196 (2020), 111357, https://doi.org/10.1016/j.colsurfb.2020.111357.
[51] T. Satoh, M. Nishida, H. Tsunoda, T. Kubo, Expression of glutathione S-transferase pi (GST-pi) in human malignant ovarian tumors, Eur. J. Obstet. Gynecol. Reprod. Biol. 96 (2001) 202–208.
[52] A. Sau, F. Pellizzari Tregno, F. Valentino, G. Federici, A.M. Caccuri, Glutathione transferases and development of new principles to overcome drug resistance, Arch. Biochem. Biophys. 500 (2010) 116–122, https://doi.org/10.1016/j.abb.2010.05.012.
[53] D.S. Backos, C.C. Franklin, P. Reigan, The role of glutathione in brain tumor drug resistance, Biochem. Pharmacol. 83 (2012) 1005–1012, https://doi.org/10.1016/j.bcp.2011.11.016.